

Sim-to-Real Transfer of Deep Reinforcement Learning Agents for Online Coverage Path Planning

Arvi Jonnarth^{1,2}, Ola Johansson¹, Michael Felsberg¹

¹Linköping University, ²Husvarna Group
{name.surname}@liu.se

Abstract

Sim-to-real transfer presents a difficult challenge, where models trained in simulation are to be deployed in the real world. The distribution shift between the two settings leads to biased representations of the dynamics, and thus to sub-optimal predictions in the real-world environment. In this work, we tackle the challenge of sim-to-real transfer of reinforcement learning (RL) agents for coverage path planning (CPP). In CPP, the task is for a robot to find a path that covers every point of a confined area. Specifically, we consider the case where the environment is unknown, and the agent needs to plan the path online while mapping the environment. We bridge the sim-to-real gap through a semi-virtual environment, including a real robot and real-time aspects, while utilizing a simulated sensor and obstacles to enable environment randomization and automated episode resetting. We investigate what level of fine-tuning is needed for adapting to a realistic setting, comparing to an agent trained solely in simulation. We find that a high inference frequency allows first-order Markovian policies to transfer directly from simulation, while higher-order policies can be fine-tuned to further reduce the sim-to-real gap. Moreover, they can operate at a lower frequency, thus reducing computational requirements. In both cases, our approaches transfer state-of-the-art results from simulation to the real domain, where direct learning would take in the order of weeks with manual interaction, that is, it would be completely infeasible.

Introduction

A practical limitation for training machine learning models is the need for large amounts of real-world data, which is tedious and time-consuming to collect. In particular, training reinforcement learning (RL) agents for robotics from scratch requires access to the robot for the full duration of the training process. Meanwhile, during the early training phase, the agent is more likely to make mistakes that may damage the hardware or require human supervision for resetting the episodes. Instead, learning in simulation presents an attractive alternative (Jonnarth, Zhao, and Felsberg 2024). However, due to differences in the dynamics between the simulation and the real world, transferring a model from simulation to reality is challenging. Prior work reduce the sim-to-real gap by improving the simulation, e.g. by injecting realistic noise (Kaufmann et al. 2023; Zhao et al. 2020),

applying domain randomization (Muratore et al. 2021; Tobin et al. 2017), or through meta learning (Arndt et al. 2020; Nagabandi et al. 2019). Our goal is to transfer, for the task of coverage path planning (CPP), the state-of-the-art performance of models trained in simulation to real environments, by fine-tuning in a realistic setting.

In CPP, the task is to find a path that covers all of the free space of an environment. If the environment is known, an optimal path can be planned offline (Huang 2001). If it is unknown, the path has to be planned online during mapping of the environment, e.g. by a robot, and an optimal path cannot be found in the general case (Galceran and Carreras 2013). CPP has found its uses in many robotic applications, such as lawn mowing (Cao, Huang, and Hall 1988), vacuum cleaning (Yasutomi, Yamada, and Tsukamoto 1988), search-and-rescue (Jia et al. 2016), and exploration (Xu et al. 2022).

When training reinforcement learning models in real time on physical robots, additional considerations need to be accounted for compared to training in simulation. (1) There exists a mismatch between the real and simulated robot kinematics, dynamics, and sensing, such as slippage and noisy localization. This leads to different transition probabilities in the real world, where the predicted actions based on simulation may be suboptimal. (2) Due to inertia and latencies in the system, the dynamics are non-Markovian (Haarnoja et al. 2018b). This violates the common assumption that the Markov property holds. (3) Since the robot keeps moving during the various computations in the training process, the state observed by the agent is not perfectly aligned with the true state. This introduces a delay, where the agent predicts actions based on outdated observations of the environment. In this work, we address these problems.

To smoothen the transition into the real world, we use a real robot in a semi-virtual environment, utilizing a highly accurate positioning system in an indoor planar setting, with a simulated sensor and obstacles. This introduces the previously mentioned real-time aspects of reinforcement learning in a controlled manner, while allowing flexibility in utilizing automated episode resetting and varying training environments without having to physically construct them. By fine-tuning and evaluating CPP policies in this semi-virtual setting, we can draw conclusions about how we expect similar policies to generalize to fully realistic environments.

To reduce latency in the training process, we perform model updates in parallel with the action and state selection (Yuan and Mahmood 2022), and perform all computations on on-board hardware. We utilize soft actor-critic learning (Haarnoja et al. 2018a) for its sample efficiency and its efficacy on continuous action spaces. To account for the non-Markovian dynamics in a lightweight manner, we include past actions in the observation space. Finally, to reduce the mismatch between the simulated and real kinematics, we measure the real-world linear and angular accelerations as well as action delay, and incorporate them into the simulation. We find that a high inference frequency enables first-order Markovian policies to transfer to a real setting. By introducing delays and action observations, higher order Markovian models can be fine-tuned to further reduce the sim-to-real gap. Moreover, these models can operate at a lower frequency, thus reducing the computational requirements for deployed systems.

Our contributions can be summarized as follows:

- We propose to divide the sim-to-real problem into two steps with an intermediate case of a real robot in a virtual environment.
- We show that this division enables a transfer of state-of-the-art RL policies for CPP from simulation to the real robot.
- We propose to perform data collection and model updates in parallel, which enables real-time fine-tuning online without a separate system or stopping the robot for model updates.
- We evaluate the effects of inference frequency and fine-tuning on the performance of the real robot.

Related Work

This paper relates to coverage path planning, transferring models from simulation to the real world, and online RL in real time. We summarize the related work below.

Coverage path planning methods can roughly be categorized as planning-based or learning-based. *Planning-based* methods include decomposition methods, which divide the area into cells based on e.g. boustrophedon cellular decomposition (BCD) (Choset and Pignon 1998) or Morse decomposition (Acar et al. 2002), where each cell is covered with a pre-defined pattern. Grid-based methods, such as Spiral-STC (Gabriely and Rimon 2002) and the backtracking spiral algorithm (BSA) (Gonzalez et al. 2005), discretize the area into even smaller cells, e.g. squares, with a similar size to the agent. Then, a path is planned based on motion primitives connecting adjacent cells, i.e. to move up, down, left, or right on the grid, such that each cell is visited at least once. Frontier-based methods plan a path to a chosen point on the frontier, i.e. on the boundary between covered and non-covered regions. The choice of frontier point can be based on different aspects, such as the distance to the agent (Yamauchi 1997), the path of a rapidly exploring random tree (RRT) (Umari and Mukhopadhyay 2017) or the gradient in a potential field (Yu et al. 2021). *Learning-based* methods apply machine learning techniques, typically in combination

with planning-based methods, to find coverage paths. Reinforcement learning is the most popular paradigm due to the sequential nature of the task. Chen et al. (2019) use RL to find the order in which to cover the cells generated by BCD. Discrete methods (Piardi et al. 2019; Kyaw et al. 2020) use RL to learn which motion primitives to perform. RL has also been combined with frontier-based methods, either for predicting the cost of each frontier point (Niroui et al. 2019), or for learning the control signals to navigate to a chosen point (Hu et al. 2020). In contrast, Jonnarth, Zhao, and Felsberg (2024) propose to learn continuous control signals end-to-end from a built map and sensor data. In our work, we adopt this approach to transfer agents from simulation to a real setting. To the best of our knowledge, we are the first to do so for end-to-end RL policies in CPP.

Sim-to-real transfer. Transferring from simulation to the real world is challenging due to mismatch in both sensing and actuation (Zhao, Queralta, and Westerlund 2020). Prior work has approached this challenge by different means. Domain randomization has been utilized to randomize physical parameters in simulation, such as mass and joint damping (Muratore et al. 2021), or to randomize textures and lighting in the image domain (Tobin et al. 2017). Other works introduce perturbations in the sensing and actuation (Zhao et al. 2020). Meta learning methods aim to quickly adapt to new unseen tasks from a wide variety of training task, such as adapting to the real world from simulation (Arndt et al. 2020; Nagabandi et al. 2019). Another approach is to learn from expert demonstrations through imitation learning (Yan et al. 2017), which has previously been applied to coverage path planning (Hu et al. 2020). When it comes to robot control, Niroui et al. (2019) deploy an RL policy for CPP trained in simulation on a differential drive robot without fine-tuning. The policy predicts the next frontier node, where a separate non-learned module navigates to it, thus being less affected by misaligned kinematics between simulation and reality. Kaufmann et al. (2023) transfer a lightweight RL control policy using a pre-trained perception system for first-person-view drone racing, utilizing empirical noise models to improve the fidelity of the simulator. They collect perception and dynamics residuals in the real world based on a highly accurate positioning system, which they use to augment the simulation. In contrast to these works, we fine-tune our model online in the real world.

Online RL. Compared to turn-based and simulated environments, where the time for action selection and policy updates are assumed to be zero and the next state can be advanced to in an instant, online RL in the real world presents new challenges where these assumptions do not hold. The core idea in the literature for accounting for this discrepancy is to parallelize aspects of the environment interactions and the model training. Bakker et al. (2006) explore *quasi-online reinforcement learning*, where a model of the environment is built online and in parallel to training the policy based on the built environment model. Ramstedt and Pal (2019) propose *real-time reinforcement learning*, where the action selection occurs in parallel with the state selection. Concretely, given the current state and action to be taken, the agent and environment compute the

next set of state and action concurrently. This approach takes into account the time for action selection by delaying the observed state by one time step. However, it does not consider the time for model updates, which is typically much larger. Other works (Haarnoja et al. 2019; Wang, Vasan, and Mahmood 2023) distribute the model training for soft actor-critic (SAC) (Haarnoja et al. 2018a) to a separate system, while performing only the lightweight action and state selections on the on-board target hardware. This allows the data collection to be executed independently from the model updates, where the policy and replay buffer are periodically synchronized. Yuan and Mahmood (2022) employ a similar approach, but they run everything on a single edge device. They divide the training process into separate processes for the action selection, state selection, batch sampling, and gradient computation. We follow this approach. However, in our experimental setup, the action selection and batch sampling were much faster than the state selection and gradient computations, so we only use two threads in order to reduce complexity and communication overhead.

Background

In this section, we first formulate the CPP problem as a partially observable Markov decision process, and then briefly describe the approach by Jonnarth, Zhao, and Felsberg (2024), which we use to train RL agents for CPP.

Problem Formulation

We aim to transfer an RL agent trained in simulation to the real world, in the task of online coverage path planning in unknown environments. The task is for the agent to simultaneously map the *a priori* unknown environment geometry, while finding a path that covers all of its free space. A point in the free space is considered covered when the distance to the center of the agent is less than the coverage radius d , and the point is in the field-of-view of the agent. The coverage radius may be smaller or equal to the agent radius r as in the *lawn mowing problem*, or larger than r as in the *exploration problem*. For mapping the environment, the agent is equipped with a ranging sensor, which is used to add obstacle detections to a global map.

We formulate the task as a partially observable Markov decision process (POMDP), consisting of an agent that predicts actions in an environment such as to maximize a reward function. In discrete time steps $t \in \{1, \dots, T\}$, the agent predicts actions $a_t \sim \pi(a_t|o_t)$ according to policy π , based on observations o_t of the state s_t . The policy is a neural network that predicts continuous control signals a_t for the agent. Subsequently, the agent receives a new observation and reward $o_t, r_t \sim p(o_t, r_t|s_t, a_{t-1})$ from the environment, where $s_t \sim p(s_t|s_{t-1}, a_{t-1})$. The goal for the agent is to maximize the expected discounted reward $\mathbb{E}(\sum_{t=1}^T \gamma^t r_t)$, with discount factor γ .

In our particular problem, the state s_t includes the full environment geometry with all obstacles, the set of points that have been covered, as well as the pose of the agent. However, the agent only has information about what it has observed, so the observation o_t consists of the part of the

environment that has been mapped until time step t , along with covered points, agent pose, and sensor data. In the setting with a real robot, the first order Markovian property is not fulfilled, due to the dynamics including inertia and momentum. The usual approach to augment previous states in the current one becomes infeasible if the motion is implicitly represented by the agent-centered environment maps. Thus higher-order effects lead to model errors that need correction in subsequent steps.

Reinforcement Learning of Coverage Paths

In this section, we summarize the approach presented by Jonnarth, Zhao, and Felsberg (2024) for learning CPP with RL, in terms of observation space, action space, reward function, and model architecture.

Map observation. In order to represent the environment, covered regions and detected obstacles are recorded in the form of global grid-like 2D maps. To represent large regions as input to the agent, multiple local maps are used with varying scales, each with the same grid size. The maps contain increasingly larger crops of the local area, with decreasing resolution. The finest scale shows detailed information near the agent, while the coarsest scale contains the largest area at a low resolution. In addition to coverage and obstacle maps, multi-scale frontier maps are also recorded. The frontier is the boundary between covered and non-covered space, which allows the agent to easily plan paths towards non-covered regions. All maps are represented as egocentric maps, that is, they are aligned such that the agent is in the center facing upwards.

Sensor observation. To detect obstacles, the agent is equipped with a simulated light detection and ranging (lidar) sensor, which measures distances in fixed angles relative to the agent. When obstacles are detected, they are added to the obstacle map based on the known global pose of the agent. The lidar distances are included in the observation space after normalization to $[0, 1]$.

Action space. We consider a differential drive wheeled robot, which is controlled by two separately driven wheels. The agent predicts the linear and angular velocities v and ω for the robot. In contrast to the cited work, we convert them to angular velocities ω_R and ω_L for the right and left wheels,

$$\omega_R = \frac{v}{r_w} + \frac{\omega b}{2r_w}, \quad \omega_L = \frac{v}{r_w} - \frac{\omega b}{2r_w}, \quad (1)$$

where r_w is the wheel radius and b is the distance between the wheels.

Reward function. In addition to a coverage reward term, Jonnarth, Zhao, and Felsberg (2024) found it necessary to include a total variation (TV) reward that penalizes variations in the coverage map, such as excessive boundaries. By reducing the total variation, the agent learns to cover the area in a more compact manner, reducing leftover holes in the coverage map, and thus, allows for complete coverage. In total, four reward terms are used: a coverage reward R_{area} , a TV reward R_{TV} , a collision reward R_{coll} , and a constant reward R_{const} . The coverage reward is written as

$$R_{\text{area}} = \lambda_{\text{area}} \frac{A_{\text{new}}}{2rv_{\text{max}}\Delta t}, \quad (2)$$

where λ_{area} is a scaling factor, A_{new} is the newly covered area, v_{max} is the maximum speed of the robot, and Δt is the time step size. The denominator is the largest possible area that can be covered in a time step and ensures that the reward is normalized to $[0, \lambda_{\text{area}}]$. The TV reward is written as

$$R_{\text{TV}}(t) = -\lambda_{\text{TV}} \frac{V(C_t) - V(C_{t-1})}{2v_{\text{max}}\Delta t}, \quad (3)$$

with scaling factor λ_{TV} , where C_t is the coverage map at time t , and V is the total variation

$$V(x) = \sum_{i,j} \sqrt{|x_{i+1,j} - x_{i,j}|^2 + |x_{i,j+2} - x_{i,j}|^2}. \quad (4)$$

Finally, the agent is penalized by a negative obstacle collision reward R_{coll} on impact, and a constant negative reward R_{const} is given each time step. Each episode is terminated when a goal coverage has been reached, or after $\tau = 1000$ consecutive steps without new ground being covered.

Model architecture. To process the multi-scale maps together with the sensor data, a scale-grouped convolutional neural network (SGCNN) is used, which has shown to be superior to a standard CNN or MLP (Jonnarth, Zhao, and Felsberg 2024). It consists of a map feature extractor g_m , a sensor feature extractor g_s , and a fusing module g_f . The map feature extractor groups the maps by scale and processes them separately using grouped convolutions, while the sensor feature extractor and fusing module consist of fully connected layers. The control signal predictions are given by

$$(v, \omega) = g_f(g_m(M_c, M_o, M_f), g_s(S)), \quad (5)$$

where M_c , M_o , and M_f are the multi-scale coverage, obstacle, and frontier maps respectively, and S is a vector of the observed normalized lidar distance measurements.

Transferring CPP Agents to the Real World

The approach described in the previous section produces CPP agents with state-of-the-art performance in simulation. Obviously, one could train the same agent directly in the real environment. However, this would require training with manual interaction in the order of weeks to months. In this section, we describe our proposed approach, which allows to transfer the model trained in simulation to the real robot.

Learning CPP on the Real System

Even if we will not train the agent from scratch in the real setting, we need to be able to fine-tune the transferred system by RL. In common RL-libraries, such as stable-baselines3 (Raffin et al. 2021), tianshou (Weng et al. 2022), and spinningup (Achiam 2018), the data collection and model updates are performed serially. While this is feasible in simulation and turn-based environments where the environment can be paused during model updates and time can be advanced instantly to the next state after action selection, it is not practical for real-time robotic applications where the agent is trained online.

In this case, we need to wait after action selection to observe the next state, while the execution remains idle. After the environment interaction, a batch is sampled from the

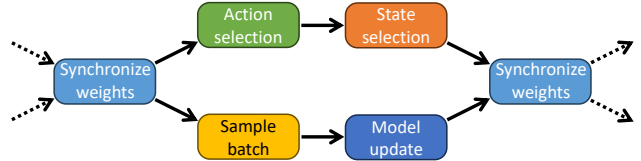


Figure 1: During online training we perform environment interactions (top) and model training (bottom) in parallel.

replay buffer, gradients are computed, and the model is updated. However, this takes time, which is not negligible, especially on low-performance edge devices and embedded systems. During the gradient update step, the robot keeps following its previous action. As a result, the agent ends up in a state which deviates from the recorded one used for action selection. Following previous work (Haarnoja et al. 2019; Yuan and Mahmood 2022), we perform the model updates in parallel with the data collection, utilizing computational resources which would otherwise remain idle while waiting for the next state.

The training process can be divided into four main computational steps, where the respective measured times are given in Table 1:

(1) Action selection: Given the current observation, we sample an action from the policy. This corresponds to a forward pass of the policy network.

(2) State selection: After sampling an action, the control signals are sent to the robot platform, and the new state is observed. In simulation, this would occur instantly, while in the real world we need to let time pass to observe how the action affected the environment. After state selection, the reward is computed, and the action, previous state, new state, and reward are added to the replay buffer.

(3) Batch sampling: A training batch is sampled from the replay buffer.

(4) Model update: Gradients are computed based on the training batch, and the model weights are updated. This is the most computationally intensive part.

Step	(1)	(2)	(3)	(4)	Overhead
Time	12 ms	450 ms	15 ms	80 ms	38 ms

Table 1: Measured times of the RL-step on the real system. Timing for (2) is application dependent, and chosen based on the optimal training step size. The overhead effectively becomes part of (1) resulting in an action delay of 50 ms.

Since the action selection and batch sampling were fast compared to the state selection and gradient computations, we only use two threads to reduce overhead and complexity. Our computational graph is shown in Figure 1, which consists of an environment interaction thread (top) and a model update thread (bottom). Since both threads interact with the replay buffer, we use a mutex to avoid conflicts. Luckily, the

the environment interaction thread adds an entry at the end of the cycle, while the model update thread samples from it early, so there is a low chance that they block each other.

Since the model update thread modifies the weight tensors during a large portion of the runtime, i.e. both during the backward pass to update the gradients and during the optimizer step to update the parameters, a mutex is not feasible as it would block execution too often. Instead, we keep a copy of the model, which is only accessed by the model update thread. The weights are synchronized when both threads have finished.

With this approach, both the environment interaction and the model update can be performed multiple times before model synchronization. This is useful when the computation time for the model update exceeds that of the action and state selection. In this case, the number of environment interaction steps should be chosen to match the computation time for the model update. Meanwhile, if the model update is fast compared to the environment interaction, multiple updates can be performed during one environment interaction step, which was the case in our experiments.

Apart from the four main computational steps, the time for simulating the sensor, creating the observation, and synchronizing the weights results in additional overhead. This effectively becomes part of the action selection as the overhead delays the observed state, and results in an *action delay*.

Smoothing the Sim-to-Real Gap

With the approach in the previous section, we could directly move to a real setting *in-the-wild*. However, this would make training and fine-tuning cumbersome as manual interaction would be required to supervise the training process. In order to fully automatically (continue to) train the system, we propose to use a semi-virtual setup, see Figure 2. In this setup, we use the real robot with its kinematics and dynamics, but simulate its lidar sensor and obstacles, and localize the robot using a positioning system. The environment, including obstacles and coverage, e.g. from mowing, is visualized by a projection onto the ground.

The main purpose of using such an environment is to evaluate, in a controlled manner, the ability of the learning algorithm to generalize to a real robot in a real-time setting. Furthermore, the considered RL approach is robust to sensing and localization noise, and can be extended to the case of unknown pose, e.g. by estimating the pose using an off-the-shelf SLAM method (Jonnarth, Zhao, and Felsberg 2024). Thus, using our semi-virtual environment, we can draw conclusions about how we expect similar policies to generalize to fully realistic settings.

As mentioned, this semi-virtual setup enables fully automatic RL with the real robot. In particular, if the robot would drive towards one of the walls, both the robot and the environment can be moved back to the middle of the room. Furthermore, since we can automatically change or generate new environments each episode, we can train general CPP policies for completely unseen environments, and not just for a single fixed environment. Finally, the setup can also be used for fully automatic benchmarking of the learned model.



Figure 2: Picture of the robot having covered an environment with four obstacles.

To further smoothen the sim-to-real gap, we improve the fidelity of the simulator by taking into consideration the latencies induced by inertia and action delay. We measure the maximum linear acceleration, maximum angular acceleration, and action delay of the real system, and include these aspects in the simulated kinematics and dynamics.

To account for higher-order Markovian dynamics, we include information from previous time steps in the observation space. While the common approach is to stack several previous observations (Haarnoja et al. 2019; Mnih et al. 2013), it is less feasible in our setting for multiple reasons. (1) Since the pose is embedded in the egocentric maps, rapid rotations significantly alter the observed state, making it difficult to learn the dynamics. (2) It significantly increases the model size and processing time, which are critical aspects for real-time applications. (3) It severely limits the replay buffer size, as the map observations are fairly large. Instead, we use a history of the previous actions (Haarnoja et al. 2019; Mnih et al. 2013), which is lightweight and avoids the listed problems, and should be sufficient for learning the dynamics of the robot. A benefit of using action observations instead of velocity estimates is that the estimates can be highly noisy. Furthermore, using action observations, the agent can learn to estimate the velocity if necessary.

Optimal Strategy for Going Sim-to-Real

When transferring the CPP model from the simulation to the semi-virtual environment, different levels of fine-tuning can be performed and the training in simulation can happen with or without higher-order dependencies in the Markov process. However, training in simulation with a first-order assumption with subsequent fine-tuning does not make too much sense because fine-tuning will always be subject to higher-order effects in the real system.

Thus, one special case is the transfer without fine-tuning, as this can use a first-order model trained in simulation with arbitrary time-steps under benchmarking. In contrast, the higher-order model implies a certain step-length during

benchmarking (and fine-tuning).

Key questions are thus:

- (1) How does the first-order model trained solely in simulation work on the real robot, dependent on the step-length?
- (2) How does the higher-order model trained solely in simulation work on the real robot and in comparison to (1)?
- (3) How does the model with fine-tuning on the real robot perform in comparison to (2) and dependent on the number of training steps?

The working hypothesis is that (3) outperforms (2), and that (1) approximates (2) with sufficiently small step size.

Experiments

In this section, we present our experimental results for transferring a state-of-the-art CPP RL policy to a semi-virtual environment.

Implementation Details

Experimental setup. The training on the physical robot is conducted using a Husqvarna Research Platform (HRP) (MIT software licence) (Husqvarna 2017): a robotic lawnmower that we equip with an Nvidia Jetson AGX Orin development kit. The wheel dimensions in (1) are $r_w = 12.25$ cm and $b = 46.5$ cm. The training algorithms, based on the stable-baselines3 implementation (MIT license) (Raffin et al. 2021), are executed on the Jetson, with control signals sent to the HRP. The experimental environment is a 12×12 meter indoor research arena. The agent receives its position from a high-precision Qualisys motion capture system (Qualisys 2023), which comprises 12 Oqus 700+ and 8 Arqus A12 cameras.

Simulation training details. We follow the training setup by Jonnarth, Zhao, and Felsberg (2024), and train the CPP policy in a simulated 2D environment. Specifically, we use the same environment parameters (also listed in the appendix), map geometries, and curriculum learning. We utilize soft actor-critic learning (Haarnoja et al. 2018b), and train for 2-8M iterations with learning rate $2 \cdot 10^{-5}$, batch size 256, replay buffer size $5 \cdot 10^5$, and discount factor $\gamma = 0.99$. We use a 360° simulated lidar field-of-view, 24 lidar rays, 3.5 m lidar range, 0.15 m coverage radius, 0.26 m/s maximum linear velocity, and 1 rad/s maximum angular velocity. To improve the fidelity of the simulator we include a 0.5 m/s^2 maximum linear acceleration, 2 rad/s^2 maximum angular acceleration, 50 ms action delay, and include the 10 latest actions in the observation. The training time ranged from 25 to 100 hours on a T4 GPU and a 6226R CPU.

Real-world training details. For the fine-tuning, we lower the learning rate to $5 \cdot 10^{-6}$ to avoid potential instability issues. In order not to give a disproportionately large weight to the first environment steps, we perform pure data collection during the first 5000 steps, i.e. without any model updates. During real-world fine-tuning we use both fixed and randomized training maps that fit within the research arena, and set the goal coverage to 99% for episode termination.

Evaluation. To evaluate the various RL policies, we measure the times T_{90} and T_{99} to reach 90% and 99% coverage, respectively. These metrics were chosen as the coverage

time is usually important in CPP tasks, and common in the literature (Xu et al. 2022). To provide additional insights, we also measure path length and accumulated rotations, which are also of interest in some applications (Chen et al. 2019). We perform the evaluation on six maps not seen during training, see the appendix.

Extended analysis. We provide an extended analysis in the appendix, including videos, learned paths, collision statistics, performance on the individual evaluation maps, average speed and the learned entropy coefficient during fine-tuning, and an ablation study for the optimal training step size. The optimal training step size was 500 ms, based on which, the state selection wait time in Table 1 was chosen. Finally, a step size of 500 ms allows us to perform 4 model updates for each environment step in the real setting.

Comparison of First-order CPP Policies

We first investigate how well policies that assume a first-order Markov process transfer to our semi-virtual environment. In this experiment, the observation space does not include any previous actions, and the policy is trained for 8M steps in a simulated environment without a limit on the linear and angular accelerations, and does not include any action delay. We evaluate the policy in simulation and in the real environment before and after fine-tuning. Since this policy does not depend on the previous action sequence, we can run it at any frequency. We evaluate it at the training frequency and as fast as possible, i.e. without waiting during state selection, which was measured to 15 ms per time step.

By comparing coverage times between simulation and reality in Table 2, we see that they are in the same ballpark, where the real results are slightly worse at the lower frequency. This is expected due to differences in kinematics and other sources of error. When increasing the inference frequency, we observe faster coverage times, even surpassing the simulation results. This is likely the case due to the fact that the agent can update its actions faster and quickly adapt to errors. Thus, it can navigate more efficiently and produce a smoother pattern.

Env	Steps	Δt	T_{90}	T_{99}
Sim	0	500	6.0	9.1
Real	0	500	7.0	10.6
Real	0	15	5.4	8.3
Real	80k	15	6.3	10.9

Table 2: **First-order policy.** Average time in minutes for reaching 90% and 99% coverage on six evaluation maps. *Env*: Evaluation environment. *Steps*: Fine-tuning steps. Δt : Inference step size (ms). Note: Training step size is 500 ms.

However, after fine-tuning, we find that the performance degrades. Our hypothesis is that as the observation includes no higher-order information, the optimal action cannot be deduced. For example, if the robot completely changes the direction of rotation, it takes some time before the new rotation takes effect. The observation may not change much,

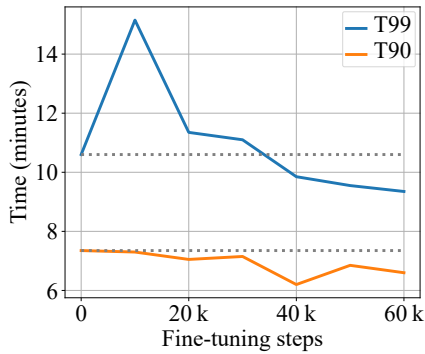


Figure 3: Average coverage times during fine-tuning on evaluation maps 1 and 2. Dashed line: No fine-tuning.

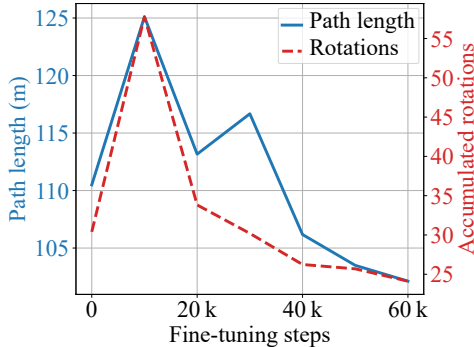


Figure 4: Average path length and accumulated full rotations during fine-tuning on evaluation maps 1 and 2.

while the optimal action does. Thus, the performance degrades initially, which may take a long time to recover from. Running the inference at a high frequency partly circumvents this problem, explaining the high performance of the model without fine-tuning. While we did not evaluate the fine-tuned policy on a lower frequency, we expect it to perform worse as in the non fine-tuning case.

Comparison of Higher-order CPP Policies

Next, we conduct a new experiment to evaluate how higher-order policies compare. We train a new model for 2M steps in simulation, where we include the past 10 actions in the observation, and limit the maximum linear and angular accelerations based on realistic estimates. Furthermore, we include the measured real-world overhead as an action delay in simulation to better align the simulation with reality. Since the 10 actions correspond to specific points back in time, we keep the inference time step the same as during training.

The new model can learn higher-order Markovian dynamics, and in Table 3 we see that it transfers well when directly deployed from simulation, surpassing the first-order model for 99% coverage under this lower inference frequency. Again, the real results are somewhat worse compared to the simulation results, as expected. In Figure 3, where we record the performance on a subset of the maps during fine-tuning, we observe that the performance degrades initially, but in

Env	Steps	Δt	T_{90}	T_{99}
Sim	0	500	5.8	8.5
Real	0	500	7.3	10.3
Real	60k	500	6.7	10.2

Table 3: **Higher-order policy.** Average time in minutes for reaching 90% and 99% coverage on six evaluation maps. *Env*: Evaluation environment. *Steps*: Fine-tuning steps. Δt : Inference step size (ms). Note: Training step size is 500 ms.

contrast to the first-order model, the agent surpasses its original performance. T_{99} degrades heavily in the early stage, while T_{90} remains more or less constant. This suggests that the agent initially sacrifices long-term planning in favour of low-level control. After it has adapted to the low-level controls, then the long-term planning also improves. Comparing Tables 2 and 3, the higher-order policy surpasses the first-order policy in both T_{90} and T_{99} at 500 ms after fine-tuning.

Furthermore, Figure 4 shows the path length and accumulated full rotations at 99% coverage. The number of rotations were computed by summing the absolute differences in heading angle in every time step. Similar to the coverage time, both metrics degrade initially, and then improve over time, surpassing the initial performance. This shows that the agent finds a more efficient path after fine-tuning. It reduces the number of turns, which take time, while it overlaps its previous path less, thus reducing the total path length.

In total, the fine-tuning took roughly 8 hours, which is only a small fraction of the weeks it would have taken to train from scratch. Note that, while training requires more computational power, such as a GPU, the computational requirements at inference time are much lower, and can even be done on a CPU (Jonnarth, Zhao, and Felsberg 2024).

Conclusions

In this paper, we transfer state-of-the-art CPP policies to a semi-virtual environment in order to reduce the sim-to-real gap. We address the three challenges of sim-to-real transfer presented in the introduction. (1) The mismatch between simulated and real dynamics is reduced by a high inference frequency and fine-tuning the model in a real setting. (2) Non-Markovian dynamics are accounted for by using action observations, and incorporating realistic accelerations and delays into the simulation. (3) Computational delays are addressed by parallelizing the environment interactions and the model updates. In our experiments, we find that training the model in simulation assuming a first-order Markov process is sufficient, as long as the inference frequency is sufficiently high. Meanwhile, a higher-order policy can be further improved through fine-tuning, and can be deployed at a lower inference frequency, which lowers the computational requirements for a deployed system.

Limitations and future work relate to accurate pose, simulated sensor data, and static environments with no moving obstacles. We discuss these further in the appendix.

Acknowledgements

This work was partially supported by the Wallenberg AI, Autonomous Systems and Software Program (WASP), funded by the Knut and Alice Wallenberg (KAW) Foundation. The computational resources were provided by the National Academic Infrastructure for Supercomputing in Sweden (NAISS), partially funded by the Swedish Research Council through grant agreement no. 2022-06725, and by the Berzelius resource, provided by the KAW Foundation at the National Supercomputer Centre (NSC).

References

- Acar, E. U.; Choset, H.; Rizzi, A. A.; Atkar, P. N.; and Hull, D. 2002. Morse decompositions for coverage tasks. *The international journal of robotics research*, 21(4): 331–344.
- Achiam, J. 2018. Spinning Up in Deep Reinforcement Learning.
- Arndt, K.; Hazara, M.; Ghadirzadeh, A.; and Kyrki, V. 2020. Meta reinforcement learning for sim-to-real domain adaptation. In *2020 IEEE International Conference on Robotics and Automation (ICRA)*, 2725–2731. IEEE.
- Bakker, B.; Zhumatiy, V.; Gruener, G.; and Schmidhuber, J. 2006. Quasi-online reinforcement learning for robots. In *Proceedings 2006 IEEE International Conference on Robotics and Automation, 2006. ICRA 2006.*, 2997–3002. IEEE.
- Cao, Z. L.; Huang, Y.; and Hall, E. L. 1988. Region filling operations with random obstacle avoidance for mobile robots. *Journal of Robotic systems*, 5(2): 87–102.
- Chen, X.; Tucker, T. M.; Kurfess, T. R.; and Vuduc, R. 2019. Adaptive Deep Path: Efficient Coverage of a Known Environment under Various Configurations. In *2019 IEEE/RSJ International Conference on Intelligent Robots and Systems (IROS)*, 3549–3556.
- Choset, H.; and Pignon, P. 1998. Coverage path planning: The boustrophedon cellular decomposition. In *Field and service robotics*, 203–209. Springer.
- Gabrieli, Y.; and Rimon, E. 2002. Spiral-STC: An online coverage algorithm of grid environments by a mobile robot. In *Proceedings 2002 IEEE International Conference on Robotics and Automation (Cat. No. 02CH37292)*, volume 1, 954–960. IEEE.
- Galceran, E.; and Carreras, M. 2013. A survey on coverage path planning for robotics. *Robotics and Autonomous Systems*, 61(12): 1258–1276.
- Gonzalez, E.; Alvarez, O.; Diaz, Y.; Parra, C.; and Bustacara, C. 2005. BSA: A complete coverage algorithm. In *proceedings of the 2005 IEEE international conference on robotics and automation*, 2040–2044. IEEE.
- Haarnoja, T.; Ha, S.; Zhou, A.; Tan, J.; Tucker, G.; and Levine, S. 2019. Learning to Walk Via Deep Reinforcement Learning. In *Proceedings of Robotics: Science and Systems*. Freiburg/Breisgau, Germany.
- Haarnoja, T.; Zhou, A.; Abbeel, P.; and Levine, S. 2018a. Soft actor-critic: Off-policy maximum entropy deep reinforcement learning with a stochastic actor. In *International conference on machine learning*, 1861–1870. PMLR.
- Haarnoja, T.; Zhou, A.; Hartikainen, K.; Tucker, G.; Ha, S.; Tan, J.; Kumar, V.; Zhu, H.; Gupta, A.; Abbeel, P.; et al. 2018b. Soft actor-critic algorithms and applications. *arXiv preprint arXiv:1812.05905*.
- Hu, J.; Niu, H.; Carrasco, J.; Lennox, B.; and Arvin, F. 2020. Voronoi-based multi-robot autonomous exploration in unknown environments via deep reinforcement learning. *IEEE Transactions on Vehicular Technology*, 69(12): 14413–14423.
- Huang, W. H. 2001. Optimal line-sweep-based decompositions for coverage algorithms. In *Proceedings 2001 ICRA. IEEE International Conference on Robotics and Automation (Cat. No. 01CH37164)*, volume 1, 27–32. IEEE.
- Husqvarna. 2017. Husqvarna Research Platform. <https://github.com/HusqvarnaResearch/hrp>. Accessed: 2024-05-22.
- Jia, D.; Wermelinger, M.; Diethelm, R.; Krüsi, P.; and Hutter, M. 2016. Coverage path planning for legged robots in unknown environments. In *2016 IEEE international symposium on safety, security, and rescue robotics (SSRR)*, 68–73. IEEE.
- Jonnarth, A.; Zhao, J.; and Felsberg, M. 2024. Learning Coverage Paths in Unknown Environments with Deep Reinforcement Learning. In *International Conference on Machine Learning (ICML)*, volume 235, 22491–22508. PMLR.
- Kaufmann, E.; Bauersfeld, L.; Loquercio, A.; Müller, M.; Koltun, V.; and Scaramuzza, D. 2023. Champion-level drone racing using deep reinforcement learning. *Nature*, 620(7976): 982–987.
- Kyaw, P. T.; Paing, A.; Thu, T. T.; Mohan, R. E.; Le, A. V.; and Veerajagadheswar, P. 2020. Coverage path planning for decomposition reconfigurable grid-maps using deep reinforcement learning based travelling salesman problem. *IEEE Access*, 8: 225945–225956.
- Mnih, V.; Kavukcuoglu, K.; Silver, D.; Graves, A.; Antonoglou, I.; Wierstra, D.; and Riedmiller, M. 2013. Playing atari with deep reinforcement learning. *arXiv preprint arXiv:1312.5602*.
- Muratore, F.; Eilers, C.; Gienger, M.; and Peters, J. 2021. Data-efficient domain randomization with bayesian optimization. *IEEE Robotics and Automation Letters*, 6(2): 911–918.
- Nagabandi, A.; Clavera, I.; Liu, S.; Fearing, R. S.; Abbeel, P.; Levine, S.; and Finn, C. 2019. Learning to adapt in dynamic, real-world environments through meta-reinforcement learning. In *International Conference on Learning Representations (ICLR)*.
- Niroui, F.; Zhang, K.; Kashino, Z.; and Nejat, G. 2019. Deep reinforcement learning robot for search and rescue applications: Exploration in unknown cluttered environments. *IEEE Robotics and Automation Letters*, 4(2): 610–617.
- Piardi, L.; Lima, J.; Pereira, A. I.; and Costa, P. 2019. Coverage path planning optimization based on Q-learning algorithm. In *AIP Conference Proceedings*, volume 2116, 220002. AIP Publishing LLC.

- Qualisys. 2023. Qualisys motion capture system. <https://www.qualisys.com/software/qualisys-track-manager/>. Accessed: 2024-05-22.
- Raffin, A.; Hill, A.; Gleave, A.; Kanervisto, A.; Ernestus, M.; and Dormann, N. 2021. Stable-baselines3: Reliable reinforcement learning implementations. *Journal of Machine Learning Research*, 22(268): 1–8.
- Ramstedt, S.; and Pal, C. 2019. Real-time reinforcement learning. *Advances in neural information processing systems*, 32.
- Tobin, J.; Fong, R.; Ray, A.; Schneider, J.; Zaremba, W.; and Abbeel, P. 2017. Domain randomization for transferring deep neural networks from simulation to the real world. In *2017 IEEE/RSJ international conference on intelligent robots and systems (IROS)*, 23–30. IEEE.
- Umari, H.; and Mukhopadhyay, S. 2017. Autonomous robotic exploration based on multiple rapidly-exploring randomized trees. In *2017 IEEE/RSJ International Conference on Intelligent Robots and Systems (IROS)*, 1396–1402. IEEE.
- Wang, Y.; Vasan, G.; and Mahmood, A. R. 2023. Real-time reinforcement learning for vision-based robotics utilizing local and remote computers. In *2023 IEEE International Conference on Robotics and Automation (ICRA)*, 9435–9441. IEEE.
- Weng, J.; Chen, H.; Yan, D.; You, K.; Duburcq, A.; Zhang, M.; Su, Y.; Su, H.; and Zhu, J. 2022. Tianshou: A highly modularized deep reinforcement learning library. *Journal of Machine Learning Research*, 23(267): 1–6.
- Xu, Y.; Yu, J.; Tang, J.; Qiu, J.; Wang, J.; Shen, Y.; Wang, Y.; and Yang, H. 2022. Explore-bench: Data sets, metrics and evaluations for frontier-based and deep-reinforcement-learning-based autonomous exploration. In *2022 International Conference on Robotics and Automation (ICRA)*, 6225–6231. IEEE.
- Yamauchi, B. 1997. A frontier-based approach for autonomous exploration. In *Proceedings 1997 IEEE International Symposium on Computational Intelligence in Robotics and Automation CIRA'97. Towards New Computational Principles for Robotics and Automation*, 146–151. IEEE.
- Yan, M.; Frosio, I.; Tyree, S.; and Kautz, J. 2017. Sim-to-real transfer of accurate grasping with eye-in-hand observations and continuous control. *Workshop on Acting and Interacting in the Real World, Advances in Neural Information Processing Systems*.
- Yasutomi, F.; Yamada, M.; and Tsukamoto, K. 1988. Cleaning robot control. In *Proceedings. 1988 IEEE International Conference on Robotics and Automation*, 1839–1841. IEEE.
- Yu, J.; Tong, J.; Xu, Y.; Xu, Z.; Dong, H.; Yang, T.; and Wang, Y. 2021. Smmr-explore: Submap-based multi-robot exploration system with multi-robot multi-target potential field exploration method. In *2021 IEEE International Conference on Robotics and Automation (ICRA)*, 8779–8785. IEEE.
- Yuan, Y.; and Mahmood, A. R. 2022. Asynchronous reinforcement learning for real-time control of physical robots. In *2022 International Conference on Robotics and Automation (ICRA)*, 5546–5552. IEEE.
- Zhao, W.; Queralta, J. P.; Qingqing, L.; and Westerlund, T. 2020. Towards closing the sim-to-real gap in collaborative multi-robot deep reinforcement learning. In *5th International conference on robotics and automation engineering (ICRAE)*, 7–12. IEEE.
- Zhao, W.; Queralta, J. P.; and Westerlund, T. 2020. Sim-to-real transfer in deep reinforcement learning for robotics: a survey. In *2020 IEEE symposium series on computational intelligence (SSCI)*, 737–744. IEEE.

Appendix

This appendix contains the evaluation maps, extended results and analysis, as well as a discussion on limitations.

Evaluation Maps

Figure 5 illustrates the six evaluation maps used to measure the performance of the CPP policies.

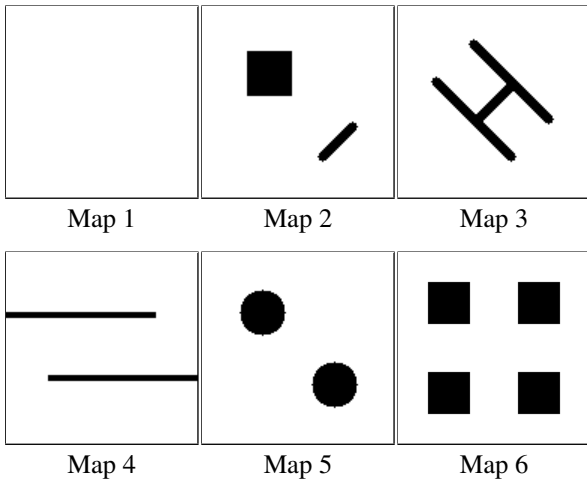


Figure 5: The six evaluation maps used in our experiments.

Learned Paths

Figure 6 shows learned paths on four of the evaluation environments, and videos can be found online.¹

Optimal Training Step Size

In Table 4, we investigate the impact of the training step size in simulation, both for first-order and higher-order policies. In both cases, 500 ms seems to be the best choice, considering 90% and 99% coverage times. Thus, we chose 500 ms for the experiments in the main paper.

If the step size is small, it may take longer to train in simulation since the computation time per step is the same. More steps are needed to complete the same number of episodes.

¹Videos are available at: <https://drive.google.com/drive/folders/1J0vpOBuRhCHOxsnAE1Vd1cZ6-qHPlvUh?usp=sharing>

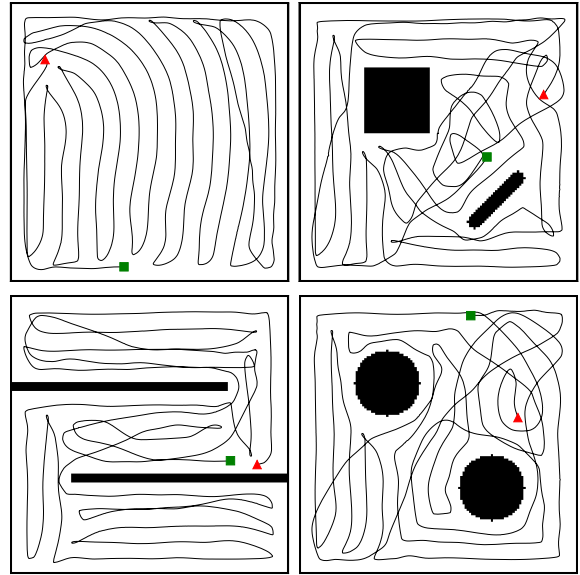


Figure 6: Learned paths showing the starting position (red triangle) and the end position (green square).

Δt	First order		Higher order	
	T_{90}	T_{99}	T_{90}	T_{99}
150	7.1	12.7	7.6	13.7
250	6.4	9.3	6.4	10.1
500	6.0	9.1	5.8	8.5
1000	6.1	9.6	6.4	9.1

Table 4: Training step size comparison (Δt in ms). T_{90} and T_{99} : Average time in minutes for reaching 90% and 99% coverage on the six evaluation maps in simulation.

In Table 4, we used the same number of training steps, which meant that the number of episodes were lower for the smaller step sizes. Meanwhile, with a lower step size, future rewards are more strongly discounted, and thus, long-term planning might be limited. It is possible that this could be remedied by tuning hyperparameters, such as the discount factor, γ . We simply used the default value of $\gamma = 0.99$ for SAC

Env	Steps	Δt	Map 1		Map 2		Map 3		Map 4		Map 5		Map 6		Average	
			T_{90}	T_{99}												
Sim	0	500	6.1	8.0	5.2	7.8	5.7	9.1	5.9	9.6	5.2	8.1	8.1	11.8	6.0	9.1
Real	0	500	5.7	9.5	6.5	10.5	6.5	9.7	9.0	10.9	6.0	9.1	8.5	13.8	7.0	10.6
Real	0	15	5.3	6.9	5.1	7.6	5.5	10.5	5.0	6.8	5.2	6.8	6.5	11.0	5.4	8.3
Real	80k	15	6.4	8.4	6.1	11.0	5.6	11.6	5.7	9.0	6.2	10.4	7.5	15.1	6.3	10.9

Table 5: **First-order policy.** Time in minutes for reaching 90% and 99% coverage. *Env*: Evaluation environment. *Steps*: Fine-tuning steps. Δt : Inference step size (ms). Note: Training step size is always 500 ms.

Env	Steps	Δt	Map 1		Map 2		Map 3		Map 4		Map 5		Map 6		Average	
			T_{90}	T_{99}												
Sim	0	500	5.6	8.6	5.7	8.7	5.2	8.2	5.3	7.6	5.2	7.3	7.7	10.3	5.8	8.5
Real	0	500	6.8	10.5	7.9	10.7	6.7	10.9	7.0	9.1	6.0	8.3	9.4	12.5	7.3	10.3
Real	60k	500	6.7	9.2	6.5	9.5	6.1	11.0	6.2	9.1	6.2	9.2	8.4	13.0	6.7	10.2

Table 6: **Higher-order policy.** Time in minutes for reaching 90% and 99% coverage. *Env*: Evaluation environment. *Steps*: Fine-tuning steps. Δt : Inference step size (ms). Note: Training step size is always 500 ms.

(Haarnoja et al. 2018a). Finally, a lower step size requires a higher number of good consecutive actions to achieve a good result, which might inhibit learning.

On the other hand, if the step size is too large, the short-term control is limited, as each action is applied over a longer time period. This requires the agent to be more precise in its actions, which makes the problem harder. A step size of 500 ms seemed to strike a good balance.

Extended Coverage Results

Tables 5 and 6 are extensions of Tables 2 and 3 in the main paper. They contain the 90% and 99% coverage times for each individual evaluation map, as well as the average times.

Average Speed

In Figure 7, we analyse the average speed of the agent during fine-tuning. The initial drop in performance is also evident here. In the initial fine-tuning phase, the agent attains a lower average speed, as a result of e.g. more collisions and many small turns, while it adjusts to the new environment dynamics. Over time, it learns to control the robot in a more efficient manner, allowing it to keep a higher average speed with less turns, which results in lower coverage times.

Learned Entropy

Figure 8 shows the learned entropy coefficient in the soft actor-critic framework (Haarnoja et al. 2018b). It increases initially, suggesting that the agent prioritizes exploration over exploitation during the distribution shift to the real world. After the initial peak, the entropy coefficient decreases, putting more emphasis on exploitation. However, it does not reach the same level as in simulation, i.e. at 0 fine-tuning steps. This either suggests that the real environment is more uncertain, or that the learning process has not entirely converged yet. It is likely a combination of the two.

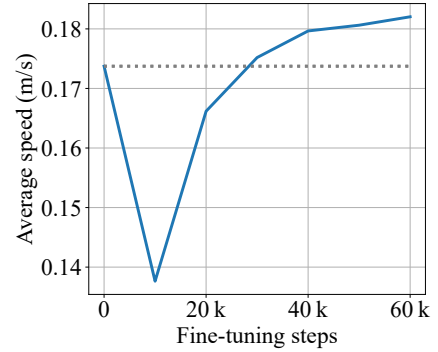


Figure 7: Average speed during fine-tuning on evaluation maps 1 and 2. Dashed line: No fine-tuning.

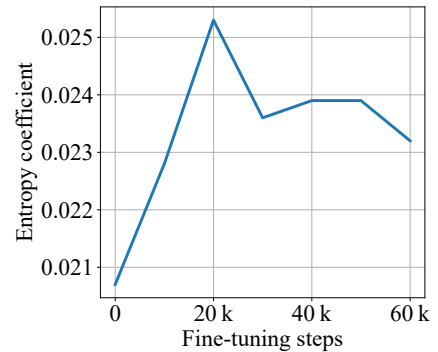


Figure 8: The learned entropy coefficient in soft actor-critic (Haarnoja et al. 2018b) during fine-tuning.

Collision Frequency

The collision frequency on the six evaluation maps in the real setting was measured to be once every 6.2 minutes, or

once every 65.4 meters, on average. However, the collisions were mainly from the side of the robot, and not head on. This is in line with the simulation results by Jonnarth, Zhao, and Felsberg (2024).

Additional Hyperparameters

In Table 7, we list additional hyperparameters used in our experiments. They are the same as used by Jonnarth, Zhao, and Felsberg (2024). Refer to the cited work for additional details on these parameters.

Parameter	Description	Value
<i>Multi-scale maps</i>		
-	grid resolution* (meters per pixel)	0.0375
-	map size** (number of grid cells)	32×32
m	number of scales	4
s	scale factor	4
<i>Reward parameters</i>		
λ_{area}	maximum coverage reward	1
λ_{TV}	total variation reward scale	1
R_{coll}	collision penalty	-10
R_{const}	constant reward	-0.1

Table 7: A list of additional hyperparameters used in our experiments. *Resolution for the finest scale, which is the same as the resolution for the full global map. **Note: this is not the size of the full environment, but rather the size of each scale in the multi-scale map representation.

Limitations

Accurate pose. The experiments are conducted with highly accurate pose estimates from an indoor positioning system, which may not be available, depending on the application. In such cases it needs to be estimated by other means, such as SLAM, which introduces higher levels of noise. Although the pose estimates in our experiments contain a low level of noise, Jonnarth, Zhao, and Felsberg (2024) show that adding high levels of localization and sensing noise does not impact performance to a significant extent. Thus, we believe that our conclusions likely extend to real environments with higher noise levels.

Sensing. The sim-to-real gap is mainly reduced with respect to robot kinematics and dynamics, while the sensor data remains simulated. This was done mainly to evaluate the sim-to-real transfer capability of the learning algorithm in a controlled manner, as stated in the main paper. Nevertheless, we believe that our conclusions likely extend to real sensors as well, for the same reason as above. Meanwhile, the sensing is omnidirectional in our experiments, which can be a strong assumption for some applications. However, the authors of the considered RL approach (Jonnarth, Zhao, and Felsberg 2024) demonstrated that it works even under non-omnidirectional sensing.

Dynamic obstacles. While dynamic obstacles are not explicitly modeled in the training framework, they can be accounted for by including, for instance, an object detector, to

update the map based on detected moving obstacles. When an object is detected, the corresponding location in the map is replaced with non-free space in the obstacle map, and when the object is no longer detected, it is replaced with free space again. This was briefly tested in our experiments, with the following results. The robot did not collide with detected obstacles, but rather it planned around them. When the objects were moved away, and the robot explored the same region again, it planned its path through that region if necessary. In future work, we have to consider such experiments more systematically.